CFA/VISHNO 2016

Un dispositif expérimental pour étudier les principes physiques sous-jacents à la production de la parole lors de l'articulation

A. Van Hirtum, R. Blandin et X. Pelorson
CNRS/Grenoble Univ., 11 rue de Mathématique, 38000 Grenoble, France
annemie.vanhirtum@grenoble-inp.fr

La géométrie du conduit vocal varie beaucoup lors de la production de la parole humaine afin d'articuler différents phonèmes. En même temps, le son est généré soit de facon aérodynamique quelque part dans le conduit vocal soit lors d'une interaction fluide-structure dans la glotte résultant dans une auto-oscillation des cordes vocales. La géométrie exacte du conduit vocal lors de l'articulation des sons de la parole est très complexe, ce qui ne facilite pas la compréhension ou le contrôle de cette géométrie. Pour ces raisons un dispositif expérimental est présenté dans le but de varier la géométrie d'une maquette de conduit vocal de facon contrôlée et avec un nombre de paramètres limités. Ainsi les consignes sont directement reliées au nombre de constrictions, au degré des constrictions et aux positions des constrictions ainsi qu'à leur variation au court du temps. Une telle approche permet non seulement de générer des données afin de caractser les phénomènes physiques observés, mais aussi de valider des modèles théoriques simplifiés ou des données issues de simulations numériques. Cette approche sera illustrée par des exemples de données acoustiques et leur analyse.

1 Introduction

The upper airway shape varies voluntary during articulation of different phoneme utterances so that sound is generated either aerodynamically somewhere in the upper airway or is due to a fluid-structure interaction resulting in auto-oscillation of the vocal folds in the larynx at the inlet of the vocal tract. Obviously, the detailed geometry of a time-varying human upper airway is extremely complicated and subject to intra- and inter-subject variability. In addition, measurement of geometrical, flow and acoustic properties on human subjects is limited and therefore not suitable for studies aiming physical understanding of sound production and propagation. Consequently, systematic physical studies often rely on simplified geometries to enhance understanding [1]. In the current work, an original setup is presented mimicking a varying vocal tract geometry during articulation using a limited amount of control parameters related to constriction degree, duration and position for up to two constrictions. Systematic variation of these parameters is expected to enhance validation of human speech production modeling since most studies consider a limited amount of static geometrical configurations which hinders general conclusions [6]. In addition, new insights in transient phenomena related to controlled time-varying geometries are expected to be gained since such data are few in literature. Consequently, quantitative measurements in relation to a controlled time-varying duct geometry potentially increases understanding of the impact of the duct's geometry on the flow and sound field. In the following, the design and realization of the setup is detailed and characterized. Next, examples of quantitative measurements are discussed in order to provide evidence to what extent complex aero-acoustic phenomena, including transient regimes, can be produced, reproduced and hence studied. The impact of the duct's geometry is shown.

2 Setup

2.1 Replica design

The design is inspired on recent work on the deformation of an a-priori uniform circular (diameter $D = 2b_0$, with b_0 the radius of the undeformed circular cross-section) elastic duct by pinching it between two parallel bars [5]. A quasi-analytical geometrical model was proposed and validated to describe the pinched duct portion based firstly on the assumption of a constant perimeter ($P \simeq 2\pi b_0$) and secondly on the assumption that each cross-section can be described as a stadium ring. The internal shape of the duct is modeled as a function of the imposed pinching effort $\mathcal{P} = 1 - b_{x_c}/b_0$ with $b_{x_c} \leq b_0$ corresponding to the minimum radius of the compressed duct. The approach results in an characteristic error of less than 4% of the duct's diameter for pinching efforts between 40% and 95%. Besides the low computational cost, the quasi-analytical duct model has the advantage to depend on a single parameter b_{x_c} defining the imposed pinching effort at position x_c. Moreover, the model holds regardless the importance of the applied constriction effort $\mathcal{P}$ (small, modest or severe pinching efforts). A pinched circular duct of length L oriented along the x-direction is illustrated in Fig. 1(a). Main geometrical parameters are indicated : undeformed circular internal radius b_0 defining perimeter P, wall thickness d, pinching position x_c, major $a(x)$ and minor $b(x)$ semi-axes of the cross-section.

The design of the setup exploits these features by aiming to control as a function of time t the position of pinching along the duct's main axis $x_c(t)$ as well as pinching effort $\mathcal{P}$ by imposing $b_{x_c}(t)$. Consequently, the pinched duct's geometry can be approximated from the time-dependent parameter set $\{b_{x_c}, x_c\}(t)$ using the geometrical duct model following the flowchart indicated in Fig. 2 and its outcome is illustrated in Fig. 1(b). The instantaneous input parameter set $\{b_{x_c}, x_c\}$ consists of the constriction position (x_c) and the minor axis at this position (b_{x_c}). Besides time-varying parameters, two constant geometrical duct parameters are given – unpinched internal radius and duct's length $\{b_0, L\}$ – as well as the internal diameter and length $\{D_l, l\}$ of the attachment portion necessary to mount the duct to the remaining of the setup. Therefore, the geometry is modeled for longitudinal x-positions in the range

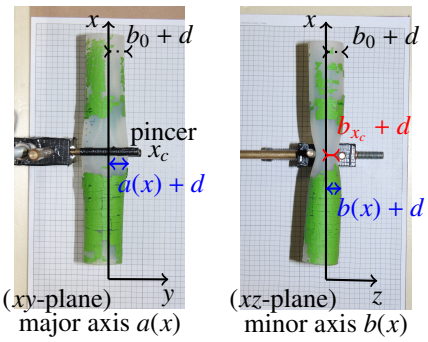

(a) principle of pinched elastic duct

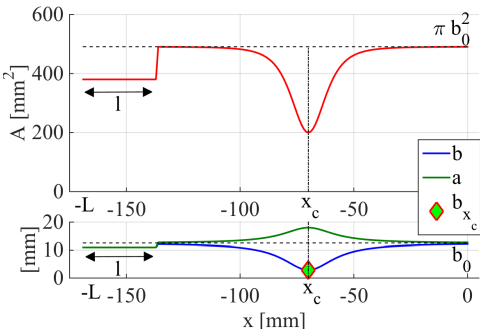

(b) duct's geometrical features ($\mathcal{P}$ = 77%)

FIGURE 1 – Illustration of pinched duct with pinching effort $\mathcal{P} = 1 - b_{x_c}/b_0$ at position x_c.

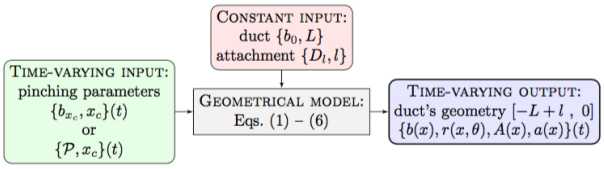

FIGURE 2 – Geometrical model flow chart.

$-L + l < x \leq 0$.

Concretely, for a pincer consisting of two parallel round bars and a duct with internal radius b_0, the minor axis at each longitudinal position $b(x)$ at time instant t is then estimated from the known input parameters as [5] :

$$b_{(x_c,b_{x_c})}(x) = b_0 - b_0 \cdot \left(1 - \frac{b_{x_c}}{b_0}\right) \cdot \left(\frac{(x - x_c)^2}{\alpha_b^2} + 1\right)^{-1}, \quad (1)$$

with for a pincer with parallel round bars of diameter 6.4 mm

$$\alpha_b(1 - \beta(x_c)) = 48\,(1 - \beta(x_c))^2 - 70\,(1 - \beta(x_c)) + 39, \quad (2)$$

$$\beta(x) = b(x)/b_0. \quad (3)$$

Once minor axis $b(x)$ is known at each longitudinal x-position, the corresponding duct's cross-section in polar coordinates (r, θ) is modelled as a piecewise function of $\theta \in [0, 2\pi]$:

$$r_b(\theta) = \begin{cases} \dfrac{b}{\sin(\theta)}, & \varphi \leq \theta \leq \pi - \varphi, \\ \dfrac{\pi}{2}\, b\, \dfrac{1-\beta}{\beta}\left[\left(\dfrac{4}{\pi^2}\left(\dfrac{\beta}{1-\beta}\right)^2 - \sin^2(\theta)\right)^{1/2} + \cos(\theta)\right], & -\varphi < \theta < \varphi, \\ \dfrac{\pi}{2}\, b\, \dfrac{1-\beta}{\beta}\left[\left(\dfrac{4}{\pi^2}\left(\dfrac{\beta}{1-\beta}\right)^2 - \sin^2(\theta)\right)^{1/2} - \cos(\theta)\right], & \pi - \varphi < \theta < \pi + \varphi, \\ -\dfrac{b}{\sin(\theta)}, & \pi + \varphi \leq \theta \leq 2\pi - \varphi, \end{cases}$$

with critical angle $\varphi(b) = \arctan \dfrac{2}{\pi}\, \dfrac{\beta}{1-\beta}$.

Other geometrical variables important for aero-acoustic applications such as the area function $A(x)$ or major axis $a(x)$ can then be expressed as a function of minor axis $b(x)$ as well :

$$A(x) = \pi b^2 + 2\pi\, b_0^2 \beta\,(1 - \beta), \quad (4)$$

$$a(x) = b + \frac{\pi}{2} b_0 (1 - \beta). \quad (5)$$

The realization of the setup for two pincers (indicated by subscript index i, the subscript is omitted in case a single pincer is used) is illustrated in Fig. 3. The realization aims to control experimental setpoints defining model input parameters $\{x_c(t), b_{x_c}(t)\}$ as well as to trace their actual values. A duct of internal radius b_0 = 12.5mm (or D = 25mm), length L = 171mm and wall thickness d = 3mm is considered. The reduced diameter of the attachment portion of length l = 33mm yields D_l = 22mm.

Concretely the time-varying geometry of the deformable portion of the duct is realized by prescribing setpoint $\{\mathcal{P}, V_z, x_c, V_x\}$ as a function of time t, where the closure or pinching degree $\mathcal{P}$ along the x-direction is set by prescribing displacements Δz along the z-direction at prescribed speeds V_x and in the same way the position of pinching x_c is set by prescribing displacements Δx at prescribed speeds V_x. The actual values of these setpoints are measured for each pincher.

2.2 Aero-acoustic facility

In order to illustrate the use of the realized setup for aero-acoustic studies involving ducts with time-varying geometry, the setup is mounted to an aero-acoustic facility as depicted in Fig. 3. Acoustic sources of different nature are encountered in speech production applications. Therefore, two aero-acoustic facilities are used allowing experiments without (acoustic facility)

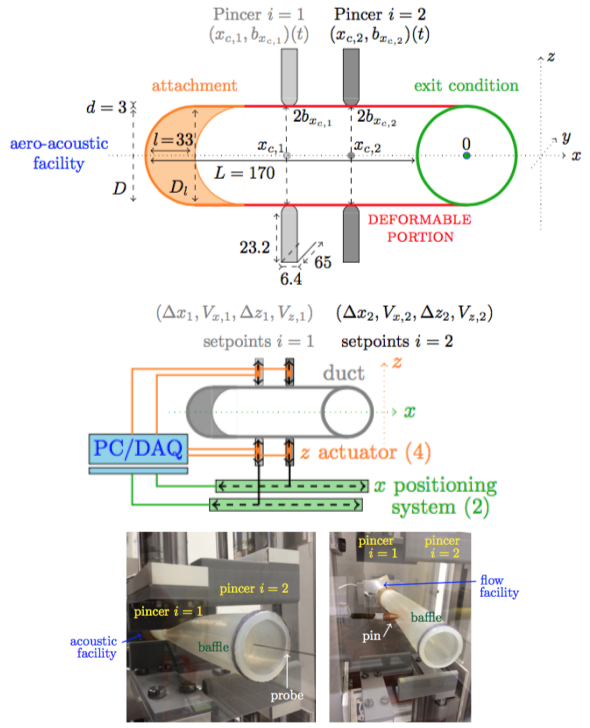

FIGURE 3 – Illustration of the realization of a deformable duct with two pincers (subscript i) [mm].

and with flow supply (flow facility). The duct's exit was fixed in a rigid flat transparent baffle (37cm×35cm and thickness 5mm, see Fig. 3) positioned parallel with the duct's exit (the chosen exit condition is *e.g.* of interest to mimic a face so that a single exit condition is considered. A multiple input and multiple output data acquisition card is used during all measurements to capture sensor data or generate signals.

To perform acoustic experiments without flow, the deformable duct was attached to an acoustic source facility (sinusoidal and white noise signals generated by a compression chamber (Monacor KU-916T) for frequency range from 0.1-4kHz) by means of a rigid connecting piece with central communication hole of diameter 2mm. Acoustic pressure $p(t)$ was measured at a fixed position inside the duct along its centerline ($x = -12$mm, $z = 0$mm) using an acoustic probe (UA 9005, diameter 1mm and length 200mm) attached to a microphone (microphone B&K 2669L and pre-conditioner B&K 5935L). The probe's position is illustrated in Fig. 3.

To perform aero-acoustic experiments with flow, the deformable duct was attached to a flow facility with settling box. The flow facility consisted of an air compressor (Atlas Copco GA7 isolated in a separated room), followed by a pressure regulator (Norgren type 11-818-987) and a manual valve so that the volume flow rate Q was controlled (4043 TSI). The replica was mounted to an upstream settling box (0.25m×0.3m×0.35m) tapered with acoustic foam (SE50-AL-ML Elastomeres Solutions) and equipped with flow straighteners in order to avoid acoustic resonances (due to the flow facility setup or settling chamber) and to homogenize the flow. Downstream the settling chamber, a uniform rigid round extension duct of diameter = 25mm (same diameter as the deformable duct) with streamwise (x-direction) length $L_u = 2$cm is placed followed by a rigid clamping piece with internal diameter = 25mm and length 1.5cm to which a rigid round downstream duct (diameter = 25mm, length $L_d = 6$cm) is attached in order to mount the deformable duct. The clamping piece contains a stretched membrane (latex sheet of thickness 0.2mm, Piercan Ltd) which was slit (center cut of 12mm) so that air could pass through it. A strong acoustic source is generated due to fluid-structure interaction when auto-oscillation of the membrane occurs mimicking vocal folds auto-oscillation during phonation [7]. Additionally, sound is generated aerodynamically downstream of the membrane when air passes through the duct.

A pressure transducer (Kulite XCS-093) was placed in a fixed pressure tap (diameter 0.4mm) immediately upstream from the membrane in order to measure the upstream pressure $P_u(t)$. The pressure downstream from the membrane inside the deformable duct $P_d(t)$ is measured by placing a pressure sensor into a pressure tap (diameter 0.4mm) which can be pinned in the duct's wall. Concretely, the pin is placed at $x = -65$mm as shown in Fig. 3.

3 Experimental evidence for influence of pinching

Experiments are performed in order to illustrate the influence of pinching by considering $\{\mathcal{P}, V_z, x_c, V_x\}$ describing the time-varying geometry of the deformable portion of the duct. In the following, typical examples are given for the setup (Fig. 3) mounted to the acoustic facility (in section 3.1) and to the flow facility (in section 3.2), respectively.

3.1 Acoustic : effect of $\mathcal{P}$, V_z, x_c and V_x

White noise excitation is applied at the inlet of the deformable tube using the acoustic facility in order to investigate the impact of the different setpoints on acoustic duct resonances [1, 2, 4] by considering the spectrogram of the acoustic pressure $p(t)$. Resonances are manually checked as well as extracted applying established signal processing techniques based on linear predictive coding.

Fig. 4 illustrates characteristic spectrograms for a variation of the pinching effort ($0 \leq \mathcal{P} \leq 97\%$) at different rates ($V_z \in \{10, 200\}$mm/s) and at different pinching positions ($x_c \in \{-26, -65, -105\}$mm). For pinching efforts $\mathcal{P} < 50\%$ spectra are determined by odd multiples of the first resonance at $F_1 \approx 475$Hz as

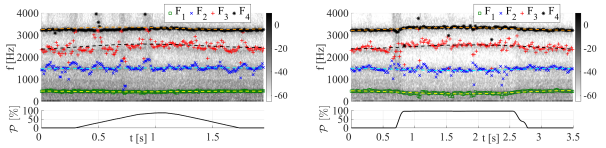

(a) $x_c = -26$mm : $V_z = 10$mm/s (left) and $V_z = 200$mm/s (right)

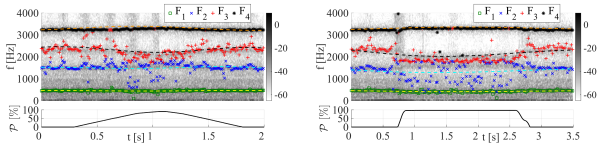

(b) $x_c = -65$mm : $V_z = 10$mm/s (left) and $V_z = 200$mm/s (right)

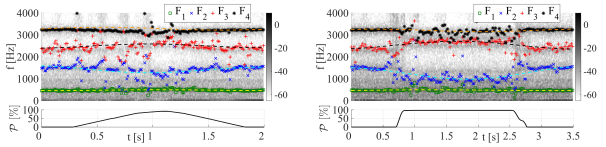

(c) $x_c = -105$mm : $V_z = 10$mm/s (left) and $V_z = 200$mm/s (right)

FIGURE 4 – Illustration of acoustic pressure spectrograms as a function of time t for setpoints $0 \leq \mathcal{P} \leq 97\%$ and $V_z \in \{10,\ 200\}$mm/s for different pinching positions x_c. Resonances F_1 ($\circ$), F_2 ($\times$), F_3 ($+$) and F_4 ($\star$) are depicted for : a) $x_c = -26$mm, b) $x_c = -65$mm and c) $x_c = -105$mm.

expected for a half open duct regardless of pinching position x_c [4]. For pinching efforts $\mathcal{P} > 50\%$ resonances shift as a function of the pinching effort $\mathcal{P}$. Moreover, the shift depends on the pinching position x_c as well. Indeed from Fig. 4 is seen that increasing the pinching effort from $\mathcal{P} = 0\%$ to $\mathcal{P} = 97\%$ increases resonance F_3 for $x_c = -105$mm ($F_3 \approx 2700$Hz) and for $x_c = -26$mm ($F_3 \approx 2450$Hz) whereas the resonance decreases for $x_c = -65$mm ($F_3 \approx 1900$Hz). In general, it is observed that the resonance frequency shift is larger for F_2 and F_3 than for F_1 and F_4. The impact of the rate of variation of the pinching effort V_z is marginal, so that as a first approximation the variation of pinching effort $\mathcal{P}$ can be considered quasi-steady. Note however, that the performance of the automated resonance detection algorithm deteriorates as the duration of the transient time associated with $\mathcal{P}$ variation decreases, *i.e.* as V_z increases, as well as when resonance values become close (*e.g.* detection of F_2 fails for $\mathcal{P} = 97\%$ at $x_c = -65$mm and $V_z = 200$mm/s as seen in Fig. 4).

Fig. 5 further highlights the influence of varying pinching position $-105 \leq x_c \leq -25$mm for a constant pinching effort ($\mathcal{P}$ set to 57% and 97%, respectively in Fig. 5(a)) as well as for a variation of pinching effort ($0 \leq \mathcal{P} \leq 97\%$ in Fig. 5(b)). It is seen from Fig. 5(b) (right) that resonance frequencies (in particular F_2 and F_3) are very sensitive to variation of both pinching position and pinching effort in the range $0 \leq \mathcal{P} \leq 97\%$.

Fig. 6 shows that for rapid variation of the pinching effort $\mathcal{P}$ at one pinching position ($x_{c,2} = -105$mm in Fig. 6) the resonance frequencies can be tuned also

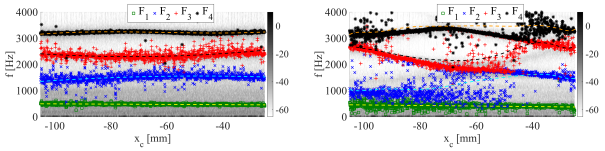

(a) constant pinching effort : $\mathcal{P} = 57\%$ (left) and $\mathcal{P} = 97\%$ (right)

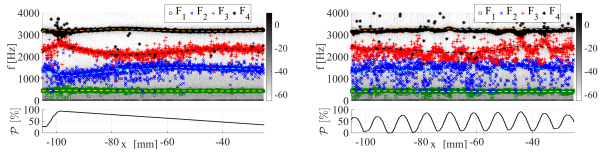

(b) varying pinching effort : $0 \leq \mathcal{P} \leq 97\%$

FIGURE 5 – Illustration of acoustic pressure spectrograms as a function of pinching position $-105 \leq x_c \leq -25$mm at velocity $V_x = 2.5$mm/s. Resonances F_1 ($\circ$), F_2 ($\times$), F_3 ($+$) and F_4 ($\star$) are depicted for : a) constant pinching effort $\mathcal{P} = 57\%$ (left) and $\mathcal{P} = 97\%$ (right) and b) varying pinching effort in the range $0 \leq \mathcal{P} \leq 97\%$ at velocity $V_z = 50$mm/s.

by imposing a pinching effort at a second pinching position ($x_{c,1} = -26$mm and $x_{c,1} = -105$mm in Fig. 6). Indeed, from Fig. 6 is easily observed that *e.g.* the

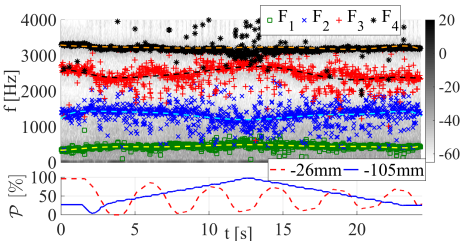

(a) $x_{c,1} = -26$mm and $x_{c,2} = -105$mm

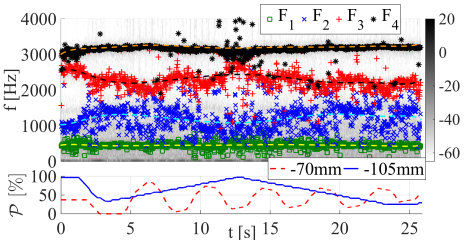

(b) $x_{c,1} = -70$mm and $x_{c,2} = -105$mm

FIGURE 6 – Illustration of acoustic pressure spectrograms as a function of time t for setpoints $0 \leq \mathcal{P} \leq 97\%$ and $V_z = 50$mm/s for pinching efforts imposed at two pinching positions simultaneously, *i.e.* $x_{c,1}$ and $x_{c,2}$ as depicted in Fig. 3. Resonances F_1 ($\circ$), F_2 ($\times$), F_3 ($+$) and F_4 ($\star$) are depicted for : a) $x_{c,1} = -26$mm and $x_{c,2} = -105$mm and b) $x_{c,1} = -70$mm and $x_{c,2} = -105$mm.

frequency spacing between F_3 and F_4 is enlarged when the additional pincer is positioned at $x_{c,1} = -70$mm compared to position $x_{c,1} = -26$mm.

The duct's response to white noise excitation shows that several strategies can be applied to vary acoustic duct resonances by varying pinching position and pinching

degree for a single pincher as well as by using two pinchers. The duct's response to a particular frequency using a sinusoidal excitation signal with known frequency is illustrated for $f_0 = 3250$Hz at pinching position $x_c = -26$mm and $f_0 = 1650$Hz at pinching position $x_c = -70$mm in Fig. 7. The repetition of the

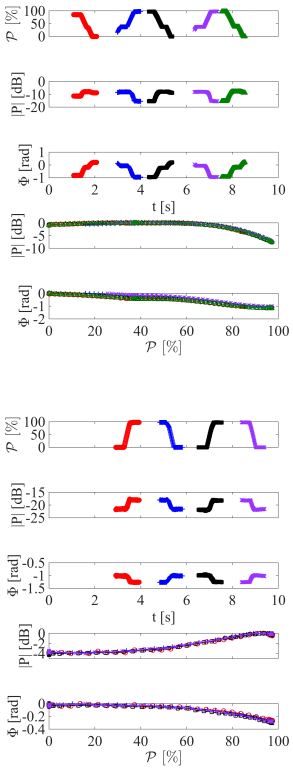

FIGURE 7 – Illustration of normalized amplitude P [dB] and phase Φ [rad] of acoustic pressure $p(t)$ as a function of time t [s] for repeated setpoints $0 \leq \mathcal{P} \leq 97\%$ and $V_z = 50$mm/s. The magnitude and phase are expressed as a function of pinching effort as well : top) $x_c = -26$mm and $f_0 = 3250$Hz and bottom) $x_c = -70$mm and $f_0 = 1650$Hz.

variation of pinching degree in the range $0 \leq \mathcal{P} \leq 97\%$, increasing as well as decreasing, is observed not to alter the associated magnitude and pressure of the measured acoustic pressure. The frequency response is further illustrated in Fig. 8. The magnitude and phase of the acoustic pressure as a function of pinching effort $\mathcal{P}$ are compared for different frequencies ($f_0 < 4$kHz) at pinching position ($x_c = -70$Hz) in Fig. 8(a). It is seen that a pronounced maximum in acoustic pressure occurs for 2200Hz at pinching degree $\mathcal{P} \approx 65\%$ and for 3250Hz at a large pinching effort $\mathcal{P} \approx 90\%$ and the phase varies in accordance. For lower frequencies ($f_0 = 1075$Hz and $f_0 - 1650$Hz) the magnitude and phase is rather flat so that their values are almost not affected by the tube's geometry, *i.e.* pinching effort $\mathcal{P}$. To further illustrate the impact of the tube's geometry on the magnitude and phase of the acoustic pressure, Fig. 8(b) illustrates their values when besides the pinching effort ($0 \leq \mathcal{P} \leq 95\%$) also the pinching position ($-105 \leq x_c \leq -26$mm)

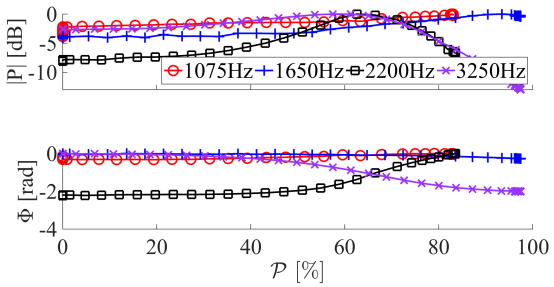

(a) $x_c = -70$mm

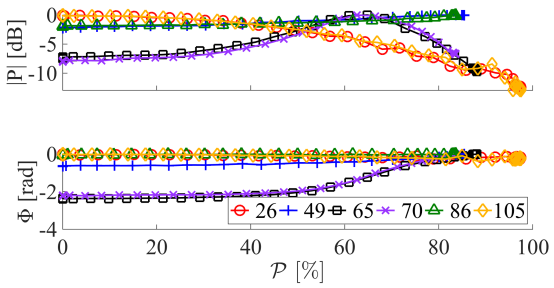

(b) $f_0 = 2200$Hz

FIGURE 8 – Illustration of normalized amplitude P [dB] and phase Φ [rad] of acoustic pressure $p(t)$ as a function of pinching effort $0 \leq \mathcal{P} \leq 97\%$ and $V_z = 50$mm/s. a) $f_0 < 4$kHz at pinching position $x_c = -70$mm and b) $f_0 = 2200$Hz at pinching positions $-105 \leq x_c \leq -26$mm.

is changed while the sinusoidal excitation frequency ($f_0 = 2200$Hz) is held constant. The position of the maximum magnitude response is observed to shift with the pinching position.

3.2 Flow : effect of $\mathcal{P}$ and x_c

Experiments using the flow facility are illustrated in Fig. 9 for different pinching efforts applied at two pinching positions $x_{c,1} = -93$mm and $x_{c,2} = -26$mm, respectively. For a uniform tube ($\mathcal{P} = 0$ in Fig. 9(a) (left)) increasing upstream pressure P_u induces auto-oscillation of the membrane and subsequent decreasing the upstream pressure ceases oscillation. During auto-oscillation the spectrogram of the pressure within the tube P_d exhibits a harmonic contents which is determined by the oscillation frequency of the membrane. Depending on the pinching position, auto-oscillation of the membrane either stops or continues, as observed when comparing pressure signals at $x_c = -26$mm for which oscillation stops (Fig. 9(b) (left)) and $x_c = -93$mm for which oscillation continues (Fig. 9(b) (right)). Besides determining the onset and offset of the oscillation, the pinching position also alters the spectral content (see Fig. 9(b) (right)) by altering the oscillation frequency and the amplitude of the harmonics. This is further illustrated by applying pinching at both $x_{c,1} = -93$mm and $x_{c,2} = -26$mm (Fig. 9(a) (right)). Indeed, the value of the oscillation frequency and associated harmonics increases as the pinching effort is increased at $x_c = -93$mm whereas oscillation stops when the pinching effort is increased

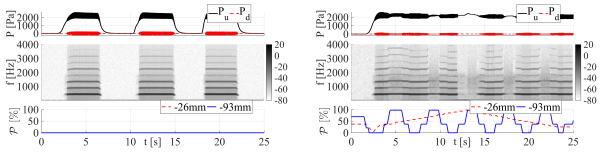

(a) uniform ($\mathcal{P}$ = 0%) and two pincers

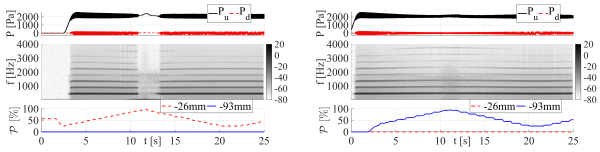

(b) one pincer

FIGURE 9 – Illustration of air pressure measured upstream from the membrane P_u [Pa] and within the tube P_d [Pa] and associated spectrogram of P_d [dB] as a function of time t [s] for different combinations of pinching efforts $\mathcal{P}$ at pinching position $x_{c,1} = -93$mm and $x_{c,2} = -26$mm, respectively.

at $x_c = -26$mm. Consequently, varying the pinching position and effort provides a strategy to alter observed oscillation features.

4 Discussion and Conclusion

A setup is presented for which the setpoints allow to control the variation of pinching positions ($x_c(t)$) and efforts ($\mathcal{P}(t)$) along a deformable tube pinched between two parallel bars. The chosen set of input parameters is particularly interesting since they have not only a clear physiological meaning (constriction degree, duration, position), but their order of magnitude can be determined on human subjects either using expensive imaging techniques such as Magnetic Resonance Imaging (MRI) scans or X-ray computed tomography (CT) scans or yet relying on alternative measurement techniques such as pressure-flow measurements [8, 3]. Moreover, it is noted that the use of a deformable tube and external pinching mechanisms avoids sharp edges. This feature might be of particular importance in order to avoid spurious aero-acoustic data since sharp edges are likely to cause unintended flow (*i.e.* flow separation or vortex shedding) and acoustic (*e.g.* sound generation and radiation) phenomena.

Examples of data obtained by mounting the setup equipped with two pincers to an aero-acoustic facility are shown. It was observed that varying pinching effort $\mathcal{P}$ and pinching position x_c alters the tube's acoustic resonances (acoustic facility) as well as the ongoing fluid-structure interaction (flow facility). A striking example of the influence of the constriction position x_c is provided by the shown experiments using the flow facility where for the same pinching effort $\mathcal{P} \approx 97\%$ the oscillation of the membrane is observed to be either inhibited ($x_c = -26$mm) or to continue with a shifted oscillation frequency and altered spectral contents ($x_c = -93$mm). In addition, examples of data using the acoustic facility show that different strategies can be used to vary the tube's resonances (F_2 and F_3 in particular). Consequently, the setup allows an accurate validation of experimental findings as a function of constant as well as time-varying tube's geometry's. Therefore, the current setup allows to study transient phenomena associated with variation of setpoints as well as with the variation of other control parameters used in the aero-acoustic facility such as the imposed upstream pressure when the flow facility is used. In addition, control strategies of acoustic resonances and auto-oscillation frequencies can be developed using the proposed setup.

Acknowledgments

This work was partly supported by EU-FET grant (EUNISON 308874).

Références

[1] G. Fant. *Acoustic theory of speech production*. De Gruyter Mouton, The Hague, The Netherlands, 1971.

[2] N.H. Fletcher and T.D. Rossing. *The physics of musical instruments*. Springer-Verlag, New York, US, 1998.

[3] Y. Fujiso, K. Nozaki, and A. Van Hirtum. Estimation of minimum oral tract constriction area in sibilant fricatives from aerodynamic data. *J. Acoust. Soc. Am.*, 138 :EL20–EL25, 2015.

[4] A. Pierce. *Acoustics. An introduction to its physical principles and applications*. Acoustical society of america, New York, 1991.

[5] A. Van Hirtum. Deformation of a circular elastic tube between two parallel bars : quasi-analytical geometrical ring models. *Mathematical Problems in Engineering*, 2015 :1–15, 2015.

[6] A. Van Hirtum and X. Pelorson. Modeling and validation of auto-oscillation onset in a constricted tube with application to phonation. *Journal of Fluids and Structures*, 58 :40–48, 2015.

[7] H. von Helmholtz. *On the Sensations of Tone as a Physiological Basis for the Theory of Music*. Longmans, Green, and Co., London, UK, 1895.

[8] D. Warren and A. DuBois. A pressure-flow technique for measuring velopharyngeal orifice area during continuous speech. *Cleft Palate J.*, 1 :52–71, 1964.